Research Square

Preprints are preliminary reports that have not undergone peer review.
They should not be considered conclusive, used to inform clinical practice,
or referenced by the media as validated information.

Investigation of an X1.5 Class Solar Flare Associated with a 3D Null - QSL System in NOAA Active Region 13006

Divya Kumari
Jai Prakash University
Pawan Kumar
pawankrchandrawanshi@gmail.com
Patna University
Sanjay Kumar
Patna University
Sadashiv .
Patna University
Alok Ranjan Tiwary
Jai Prakash University

Research Article

Keywords: Solar Flares, Magnetic Field, Extrapolation, QSLs, Magnetic Reconnection

Posted Date: July 24th, 2026

DOI: https://doi.org/10.21203/rs.3.rs-10271661/v1

License: This work is licensed under a Creative Commons Attribution 4.0 International License.
Read Full License

Additional Declarations: No competing interests reported.

Version of Record: A version of this preprint was published at Astrophysics and Space Science on September 7th, 2026. See the published version at https://doi.org/10.1007/s10509-026-04631-y.

Investigation of an X1.5 Class Solar Flare Associated with a 3D Null - QSL System in NOAA Active Region 13006

Divya Kumari[1], Pawan Kumar[2*], Sanjay Kumar[2], Sadashiv[2], Alok Ranjan Tiwary[1]

[1]University Department of Physics, Jai Prakash University, Chapra, Bihar, India.
[2*]Department of Physics, Patna University, Patna, 800005, Bihar, India.

*Corresponding author(s). E-mail(s): pawankrchandrawanshi@gmail.com;
Contributing authors: sainisanjay35@gmail.com;

Abstract

We investigate the magnetic topology and trigger mechanism of the X1.5-class flare hosted by NOAA Active region 13006 on 10 May 2022, combining multi-wavelength observations with a Non-Force-Free-Field (NFFF) extrapolation. Observations show a circular brightening and a remote brightening that evolve into corresponding circular and remote flare ribbons during the impulsive phase. GONG Hα data reveal a pre-existing arc-shaped filament within the flaring region that stays stable throughout the flare and subsequently shows signs of eruption shortly afterward. The NFFF extrapolation of the active region depicts the presence of a three dimensional (3D) null exhibiting a fan-spine structure, a filament located beneath the fan dome within the flaring kernel. The extrapolated field accurately reproduces the observed coronal morphology and demonstrates a close spatial relationship between the fan footprints and the circular ribbon. The analysis also reveals a circular quasi-separatrix layer (QSL) surrounding the fan footprints, while enhanced $|\mathbf{J}|/|\mathbf{B}|$ near the null point indicates favorable conditions for current-sheet formation and reconnection. Measurements of the photospheric magnetic flux further indicate flux cancellation beneath the fan structure during the flare, implying a gradual buildup of magnetic free energy. The flux evolution implies that the sheared arcade beneath the fan may progressively transform into a flux rope, eventually leading to eruption. We propose that the flare is triggered by slipping magnetic reconnection within the circular

QSL, leading to the initial circular brightening, followed by reconnection at the 3D null that amplifies the circular ribbon and produces the remote ribbon.

Keywords: Solar Flares, Magnetic Field, Extrapolation, QSLs, Magnetic Reconnection

1 Introduction

Solar flares represent some of the most powerful explosive events occurring in the solar atmosphere, discharging as much as 10^{32} erg of magnetic energy in a matter of minutes through magnetic reconnection. This swift conversion of energy heats the plasma, accelerates charged particles, and generates intense electromagnetic radiation that ranges from radio waves to gamma rays (Shibata and Magara 2011). Flares are frequently associated with coronal mass ejections (CMEs) and energetic particle events, positioning them as key contributors to space weather, which can have significant impacts on the near-Earth environment, satellite operations, communication systems, and power grids. Despite many years of observational and theoretical advancements, the underlying physical mechanisms that trigger flares and facilitate energy release, especially within intricate three-dimensional (3D) magnetic configurations, continue to be a vibrant field of research in solar physics (Shibata and Magara 2011; Priest 2023).

The traditional CSHKP model (Carmichael 1964; Sturrock 1966; Hirayama 1974; Kopp and Pneuman 1976) a.k.a standard flare model effectively accounts for numerous observational characteristics of eruptive flares within a two-dimensional (2D) context. Nevertheless, high-resolution data from contemporary space missions have shown that the majority of solar flares develop within inherently 3D magnetic configurations (Mandrini et al. 1996; Aulanier et al. 2000; Masson et al. 2009; Wang and Liu 2012; Li et al. 2019; Devi et al. 2020). These findings encompass circular and multiple flare ribbons, slipping ribbon movements, remote brightenings, and intricate loop connectivity, which remain inadequately addressed by 2D reconnection models. As a result, it becomes imperative to explore the 3D magnetic topologies of active regions to comprehend the initiation and progression of solar flares.

Among the various topological structures present in the solar corona, 3D magnetic null points and quasi-separatrix layers (QSLs) are regarded as optimal sites for magnetic reconnection (Prasad et al. 2018; Nayak et al. 2019; Agarwal et al. 2024; Nayak et al. 2025; Kumar et al. 2025; Kumar et al. 2026). A magnetic null point is defined by a vanishing magnetic field and generally exhibits a fan-spine topology, which includes a dome-shaped fan separatrix surface along with two spine field lines. Conversely, QSLs are areas where the connectivity of magnetic field lines changes rapidly yet continuously, resulting in significant current concentrations that promote magnetic reconnection. Relevantly, QSLs are associated with a high squashing factor value (Q, Titov et al. 2002), which quantifies the gradient in field line mapping. The intersection of QSLs gives rise to a hyperbolic flux tube (HFT), which has also been recognized as an effective site for reconnection (Titov and Démoulin 1999; Titov et al. 2002; Kumar et al. 2026). An increasing amount of observational and numerical evidence indicates

that reconnection occurring simultaneously at magnetic nulls and QSLs can elucidate many intricate flare signatures, such as circular ribbons, remote brightenings, slipping reconnection, and multi-stage energy release (Prasad et al. 2018; Nayak et al. 2019; Kumar et al. 2021; Agarwal et al. 2024; Kumar et al. 2025; Kumar et al. 2026).

Confined solar flares present a particularly significant opportunity to explore the influence of magnetic topology, as they emit considerable magnetic energy without leading to a successful eruption or CME. Their confined characteristics are typically ascribed to robust overlying magnetic fields or to specific topological limitations dictated by the coronal magnetic configuration (Wang and Zhang 2007; Yang et al. 2014; Wang et al. 2017). Gaining insight into the process of magnetic reconnection in such systems is crucial for differentiating between eruptive and confined energy-release mechanisms, as well as for enhancing our comprehension of flare triggering processes. Recent magnetohydrodynamic simulations (Prasad et al. 2018; Kumar et al. 2025; Kumar et al. 2026), constrained by data, have further illustrated that reconnection occurring at magnetic null points, in conjunction with QSLs, can replicate many observed characteristics of solar flares, underscoring the significance of these topological structures.

In this study, we investigate the potential onset mechanism of an X1.5-class solar flare hosted by NOAA active region (AR) 13006 on 10 May 2022. A previous observational study of this event conducted by Gong et al. (2024) documents the rotational motion of sunspot contributes to the development of a circular filament in the region, while the cancellation of magnetic flux initiates the flare and the subsequent eruption of the filament. In our work we advance the study by employing the observations across various wavelengths which reveal a complex system of flare brightenings and ribbons in the flaring region implying the involvement of intricate magnetic structures in the energy-release process. To explore the essential magnetic topologies within the flaring region, we reconstruct the coronal magnetic field using the non-force-free-field (NFFF) extrapolation model (Hu et al. 2008, 2010). The extrapolated magnetic field depicts the presence of a circular QSL and a 3D null, both of which are spatially associated with the observed flare brightenings — suggesting that magnetic reconnection occurring within the 3D null and the QSL played a critical role in triggering the flare and enabling the emergence of the observed flare brightenings and ribbons. These results highlight the importance of complex 3D magnetic topologies in the initiation of solar flares.

The remainder of the paper is arranged as follows. Section 2 describes the multi-wavelength observations of the flare. Section 3 provides an overview of the NFFF extrapolation model and the extrapolation of AR 13006. Section 4 elaborates the key magnetic features identified in the flaring region using NFFF extrapolation and also highlights their relationship with the observation of the flare. Lastly, in Section 5 we present a summary of the main findings of this paper.

2 Observations of the Flare

On May 10, 2022, an X1.5 class solar flare was initiated in NOAA AR 13006. The flare began at 13:50 UT, reached its peak at 13:55 UT, and concluded at 13:59 UT,

as documented in GOES observations, as shown in Figure 1. The figure presents the GOES-16 X-ray (1-8 Å channel) light curve starting at 13:30 UT to 14:30 UT on May 10, 2022, derived from the soft X-ray flux data having a temporal cadence of 1 second. The vertical dashed lines drawn with green and red colors mark the flare onset and end, respectively whereas the blue marker highlights the peak in the X-ray flux.

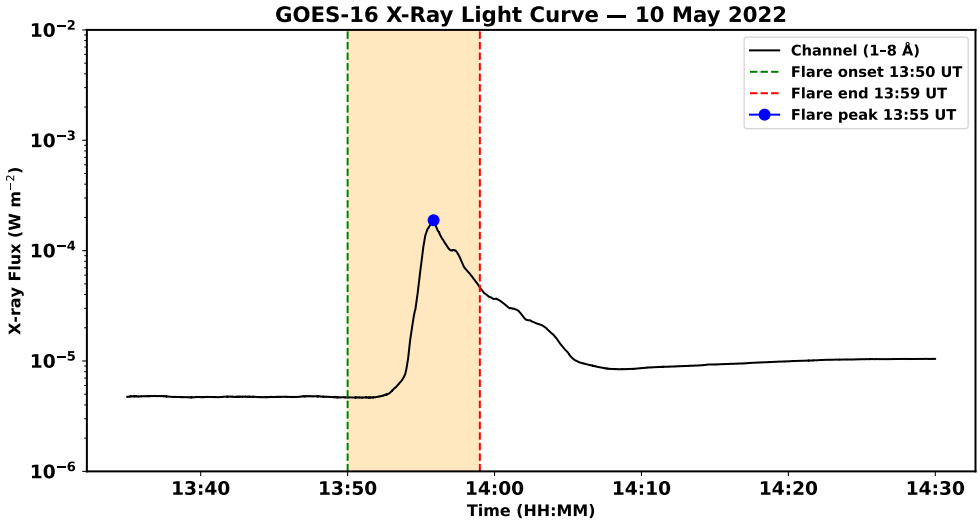


Fig. 1 GOES-16 XRS light curve of 10 May 2022 from 13:30 UT to 14:30 UT. The curve plots the X-ray flux in 1–8 Å channels as a function of time. The vertical dashed line denotes the flare onset (green) and end (red), also the blue marker identifies the magnitude of the peak flux.

Next, to investigate the flare development, we have used the multi-wavelength observations taken from the Atmospheric Imaging Assembly (AIA, Lemen et al. 2012) instrument onboard the Solar Dynamic Observatory (SDO, Pesnell et al. 2012). The AIA supplies the full disk images of the sun in ultraviolet (UV) and extreme ultraviolet (EUV) wavelengths with a time resolution of 24s and 12s, respectively. In Figure 2, we illustrate the development of flare brightenings in AIA 304 Å images. Panel (a) shows the pre-flare stage at 13:40 UT. A dark semi-circular arc-shaped structure, marked with F and indicated by a green arrow, is prominently identified in the flaring kernel. This suggests the presence of cooler materials suspended in the lower corona or transition region. Panel (b) of the figure presents the AIA 304 Å image at the flare onset, revealing F hold its position in the flaring region. Subsequently, we detect the emergence of a circular flare brightening BR1 (indicated by a yellow arrow) with a slight deformation in arc shape of F near the flare peak time (13:54 UT) in panel (c). As time advances to flare peak, BR1 gets brighten with the development of a remote brightening BR2 (marked by a white arrow) in the southwest of BR1 as illustrated in Panel (d). Notable is the F remains present with slight deformation in its shape within the flaring region throughout the flare duration.

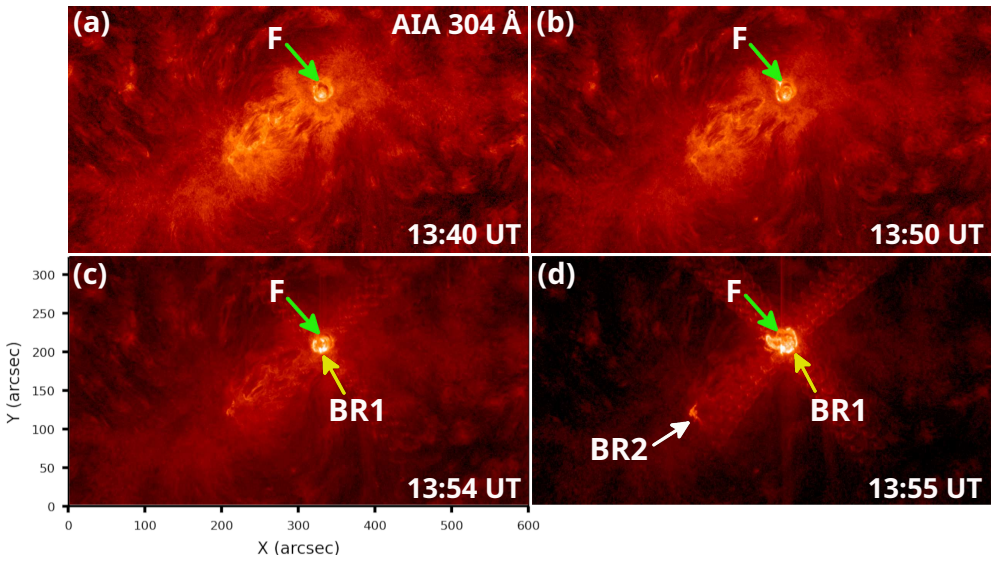


Fig. 2 Figure illustrates the flare history in the AIA 304 Å. Panel (a) corresponds to the pre-flare stage indicating the presence of a dark arc shaped structure F (pointed with a green arrow) in the flare kernel. Panel (b) presents the observation at the flare onset depicting that F holds its position. Panel (c) shows the appearance of a circular flare brightening BR1 (indicated by a yellow arrow) with slight deformation in F near the flare peak at 13:54 UT. Panel (d) shows the BR1 gets brighten over time with the development of a remote brightening BR2 (white arrow) in the southwest of BR1. Interestingly the F remains in position withing the flaring region.

Furthermore, Figure 3 illustrates the observations of the flare in AIA 131 Å (panels (a)-(c)) and 1600 Å (panel (d)). Panel (a) displays the observation recorded at 13:40 UT, which corresponds to the pre-flare phase. The green arrow highlights the existence of a dark arc-shaped structure in AIA 131 Å, akin to F observed in 2. Additionally, panel (b) shows the emergence of a subtle brightening BR1, after the flare onset at 13:51 UT. As time progresses, BR1 expands into a circular brightening around the flare peak at 13:53 UT, as illustrated in panel (c). The figure features a white dashed box that highlights the region where the flare brightenings are taking place, which is further zoomed in the inset located in the top right corner. Interestingly, the loop brightenings appear to resemble a fan-spine structure, as pointed by the pink arrows in the figure inset. Notably the fan is co-spatial with the BR1. Subsequently, we observe the development of remote brightening BR2 where the spine is anchored in photosphere (not shown in paper as the region of circular brightening is saturated in AIA 131 Å during the impulsive phase of flare) in the southwest of BR1 at 13:55 UT similar to Figure 2(d). Moreover, panel (d) of Figure 3 presents the AIA 1600 Å image at the time of flare peak, indicating the appearance of circular flare ribbon R1 (yellow arrow) and an another flare ribbon R2 (white arrow) at a remote location in the bottom-left of R1. Importantly, ribbons R1 and R2 are co-spatial with BR1 and BR2, respectively.

In quest of the magnetic feature associated with F, Figure 4 plots the GONG Hα images. Panel (a) presents the observation prior to flare onset at 13:40 UT. The

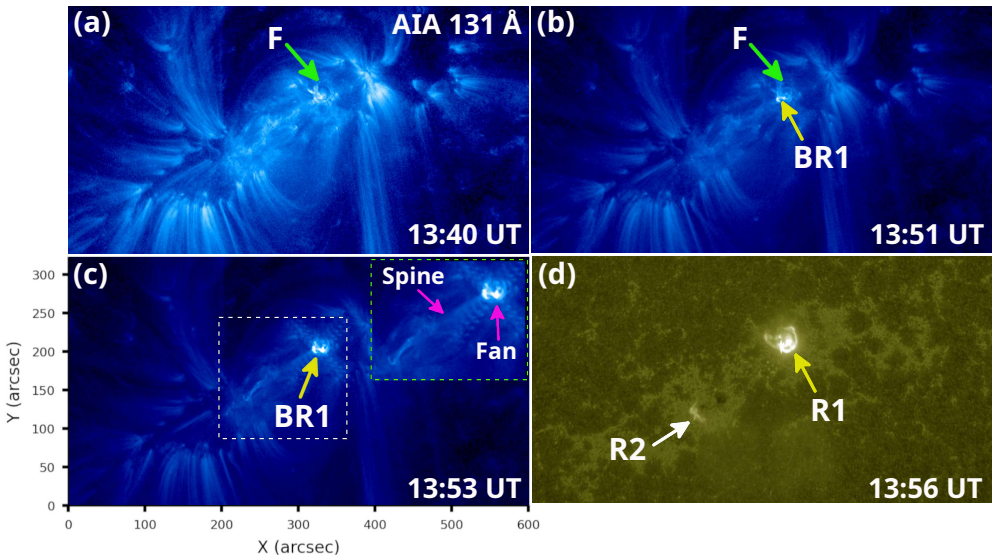


Fig. 3 Figure plots the development of flare brightenings/ribbons starting at 13:40 UT in AIA 131 Å (panels (a)-(c)) and AIA 1600 Å (panel (d)). Panel (a) shows the pre-flare observation at 13:40 UT with the presence of dark arc shaped structure F (green arrow). Panel (b) indicates the appearance of a faint brightening BR1 (yellow arrow) after the flare onset at 13:51 UT. With time, the BR1 grows as a circular brightening as shown in panel (c). The white dashed box encloses the flaring region and zoomed in figure inset. The loop brightenings in the figure inset appear to construct a fan-spine structure (pink arrows). Panel (d) displays appearance of circular flare ribbons R1 (yellow arrow) and R2 (white arrow) in AIA 1600 Å as the flare reaches to its peak.

rectangle outlined by the red solid line encompasses the area of circular brightening, which is further magnified in the inset figure (indicated by red dashed lines) for better lucidity. It also reveals the presence of a dark arc shaped structure (blue arrow) in the vicinity of circular brightening which is co-spatial to F observed in AIA 304 Å and 131 Å observations. This enables us to infer that F is a filament located in the flaring area. It is important to note that following the conclusion of the flare at 14:05 UT, F seems to have erupted from the region, as illustrated in panel (b).

The comprehensive multi-wavelength analysis of the flare indicates the appearance of two flare brightenings, BR1 and BR2, observed in both AIA 304 Å and 131 Å throughout the flare's progression. Corresponding to these two flare ribbons R1 and R2 are appeared in AIA 1600 Å. This suggests a multi-thermal response that spans from the near chromosphere and transition region to the hot coronal plasma (O'Dwyer et al. 2010; Lemen et al. 2012). In contrast to 131 Å observations, the subtle brightening occurring after the flare onset is not seen in 304 Å and 1600 Å channel. This discrepancy can be explained by the lack of faint brightening in the AIA 131 Å channel, indicating that the event either did not generate a noticeable increase in the He II line (304 Å waveband) or produced an emission measure that was below the detection limit of this channel (O'Dwyer et al. 2010; Boerner et al. 2012). Similarly, the absence of corresponding signatures in the AIA 1600 Å during the initial phase of the flare

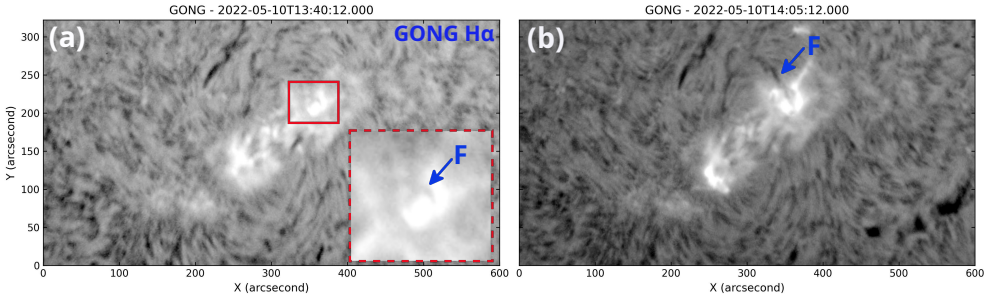


Fig. 4 Figure plots the GONG Hα images. Panel (a) identifies the presence of arc shaped filament labeled as F and pointed by blue arrow prior to flare onset at 13:40 UT. Panel (b) advocates the eruption of the F after the end of the flare at 14:05 UT.

as a counterpart to subtle BR1 indicates a comparatively modest increase in the UV continuum that contributes to this wavelength range during the energy deposition of the flare (Fletcher et al. 2011). Notably, previous studies have reported similar spatially localized brightenings that exhibit different thermal responses in Aschwanden and Shimizu (2013); Li et al. (2019); Joshi et al. (2022). In addition to this the GONG Hα observations depict the presence of arc shaped filament prior to flare onset and it seems to be erupted after the conclusion of the flare.

3 The Non-Force-Free-Field Extrapolation

To investigate the key magnetic features linked with the onset of the X1.5 class flare, we employ the NFFF extrapolation technique to evaluate the coronal magnetic field of NOAA AR 13006. This technique was modeled by Hu et al. (2008, 2010). It relies on the Minimum Dissipation Rate (MDR) principle. This principle considers that the plasma relaxes to a state that reduces energy dissipation. The relaxed state is defined by the double-curl Beltrami equation, from which the magnetic field is then derived as (Bhattacharyya et al. 2007)

$$\mathbf{B} = \mathbf{B}_1 + \mathbf{B}_2 + \mathbf{B}_3; \nabla \times \mathbf{B}_i = \alpha_i \mathbf{B}_i \tag{1}$$

where $i = 1, 2$ and 3, each $\mathbf{B}_i$ represents a linear-force-free-field associated to a twist parameter α_i. In practical, we set $\alpha_2 = 0$ and $\alpha_1 \neq \alpha_3$ in NFFF extrapolation model, that makes $\mathbf{B}_2$ a potential field. For a comprehensive description of the NFFF extrapolation model, we refer the readers to Hu and Dasgupta (2008); Hu et al. (2008, 2010).

Previous studies of Metcalf et al. (1995) and Gary (2001) suggest that the force-free equilibrium does not hold well near the photosphere. In the conventional force-free extrapolation model, a "preprocessing" technique is frequently employed to establish appropriate boundary conditions for extrapolation, allowing for the incorporation of the force present in the vector magnetogram (Wiegelmann 2008; Wiegelmann and Sakurai 2012). In particular, the NFFF extrapolated magnetic field supports the non-zero Lorentz force at lower heights and becomes almost force-free at the coronal heights

(Prasad et al. 2018). When it is compared to the standard force-free-field extrapolation model then, it is notable that no "preprocessing" technique is required in the NFFF extrapolation. This difference keeps the NFFF extrapolation model in line with the studies of Metcalf et al. (1995) and Gary (2001). In particular, previous studies carried out with the NFFF extrapolated field have successfully explained the different transient events like solar flares, coronal jets, and coronal dimming (Prasad et al. 2018; Nayak et al. 2020; Prasad et al. 2020, 2023; Kumar et al. 2025; Kumar et al. 2026) by identifying the initial key magnetic features in the AR which led to the onset of solar transient events.

3.1 NFFF extrapolation of NOAA AR 13006

We employ the photospheric vector magnetogram supplied by the Helioseismic and Magnetic Imager (HMI, Schou et al. 2012) onboard the SDO to construct the coronal magnetic field utilizing the NFFF extrapolation model. Specifically, the vector magnetic field data is selected from the `hmi.sharp_cea_720s` data series, having a pixel resolution of $0.5''$ and a temporal cadence of 12 minutes. At first, the magnetogram is remapped onto the Lambert cylindrical equal area (CEA) projection, and subsequently, it is converted into heliographic coordinates (Gary and Hagyard 1990) to obtain the magnetic field within a Cartesian grid. The extrapolation is conducted aforementioned data series at 13:48 UT (2 minutes prior to flare onset). To concentrate on the flaring region, the initial magnetogram cutout is further reduced to a grid size of 1200×644 grid points along the x and y-directions, respectively. Furthermore, 644 grid points are utilized in the z direction. This configuration represents a physical domain of approximately 432 Mm in the x direction and about 232 Mm in both the y and z directions.

4 Results

Figure 5 presents the extrapolated coronal magnetic field configuration of NOAA AR 13006 at 13:48 UT. In panel (a) demonstrates the line of sight (LOS) component (Bz) of the photospheric vector magnetic field at the bottom boundary ($z = 0$). The area encompasses by the white dashed box highlights the flaring region in which the flare brightenings are developed. Panel (b) of the figure illustrates the top view of the extrapolated field lines in the flaring region superimposed with Bz. The field lines displayed with cyan color exhibit a fan-spine geometry (white arrows), with the fan approximates a circular shape and the spine anchored in the positive plage polarities on the bottom-left at the photosphere. Subsequently to investigate the existence of a 3D null point associated with the fan-spine structure, we utilize the trilinear method for null detection developed by Haynes and Parnell (2007); Olshevsky et al. (2020). This confirms the presence of a 3D null in the flaring region, which is demonstrated with the fan-spine structure (cyan field lines). Additionally, the pink field lines traces the low-lying the magnetic arcades beneath the fan on the 3D null. These magnetic arcade (pink lines) exhibit an arc-shaped structure over the polarity inversion line akin to F observed in the Figures 2, 3 and 4. For better visualization of the fan-spine configuration, the side view of the field lines is plotted plotted in panel (c). To

investigate the presence of a pre-existing flux rope in the flaring region, we calculate the twist parameter (T_w) in the flaring domain using the following equation,

$$T_w = \frac{1}{4\pi} \int_l \alpha dl \tag{2}$$

where $\alpha = \frac{\mathbf{J}.\mathbf{B}}{|\mathbf{B}|^2}$ and dl denotes a line element (Berger and Prior 2006). It is noteworthy that T_w value exceeding 1 is not found in the flaring region. This indicates that the region of interest is devoid of pre-existing magnetic flux rope. However, we find the sheared field lines located under the fan, as shown in color pink in panel (c). We suspect that these sheared field lines may correspond to the observed filament. Panel (d) plots the magnitude of Lorentz force (L) in the extrapolation volume, suggesting the Lorentz force is non-zero at the lower heights within the flaring region.

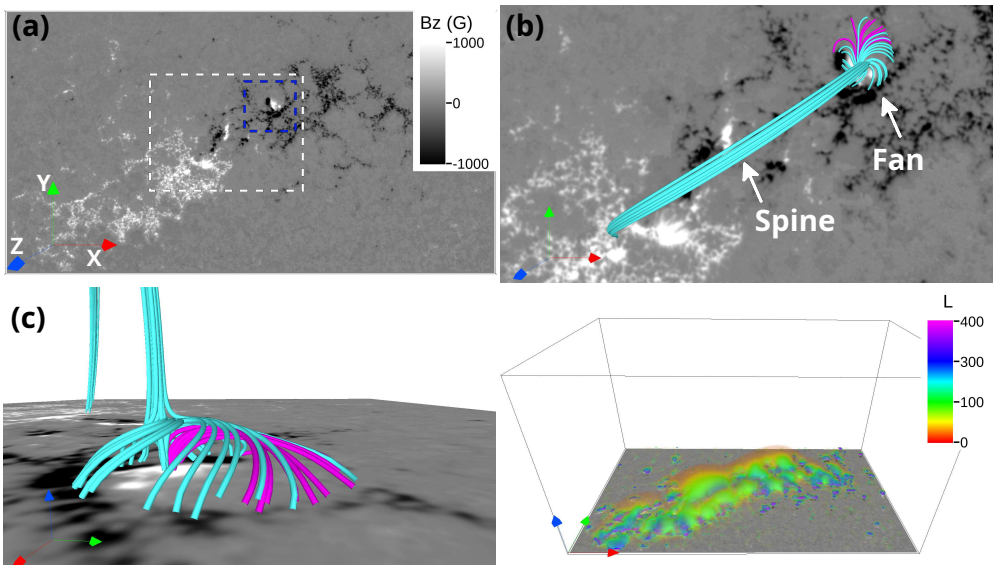


Fig. 5 The extrapolated magnetic field configuration at 13:48 UT. Panel (a) illustrates Bz component of photospheric magnetogram at the bottom boundary ($z = 0$). The white dashed box denotes the flaring region and the blue dashed box illustrates the region of circular brightening. Panels (b) and (c) show the side and top views of the extrapolated magnetic field lines overlaid with the Bz. Cyan field lines construct 3D null having circular fan spreading on right while outer spine anchored in the positive plage polarities on bottom-left. Field lines in pink color demonstrates an arc shaped filament embedded in the fan of 3D null. In panel (d) we give the volume plot of the magnitude of Lorentz force (L) in the extrapolated domain, representing the non-zero L in the flaring region at lower heights.

Next, in Figure 6(a), the field lines are superimposed with the squashing factor (Q, Titov et al. 2002) on a logarithmic scale at the bottom boundary, which signifies the gradient in the mapping of magnetic field lines. The code developed by Liu et al. (2016) is utilized for the calculation of Q. Interestingly, the foot-points of the fan of the 3D null are rooted in the regions of high $logQ$. Such high $logQ$ regions are

frequently characterized as QSLs, and are considered as the potential sites for magnetic reconnection (Titov and Démoulin 1999; Titov et al. 2002; Aulanier et al. 2006; Kumar et al. 2025; Kumar et al. 2026). Notably the QSL around the fan of 3D null exhibit a circular geometry and highlighted as QSL1 (pointed by pink arrow) in Figure 6(a). To explore the possibility of magnetic reconnection at 3D null, in panel (b), we plot the field lines of the transverse field (obtained by setting $B_y = 0$ in $\mathbf{B}$ for the cyan field lines), which illustrates the projected magnetic field lines on a y-constant plane. The projected field lines shows and X type geometry and are further overlaid with $logQ$ in y-constant plane, suggesting high value of $logQ$ at center of the X-shaped neutral point which is an indicative of strong gradient in the field line connectivity. Subsequently, we overlay the field lines of transverse field with the $|\mathbf{J}|/|\mathbf{B}|$ in the y-constant plane, as shown in panel (c). Additionally, the panel is further superimposed with the L (direction which is shown with red arrows). It is noteworthy that L is favorable to bring non-parallel field lines in close proximity leading to an increased value of $|\mathbf{J}|/|\mathbf{B}|$ (magnetic field gradient) in the proximity to the 3D null, indicating a potential development of current sheet and possibility of onset of reconnection at the 3D null (Kumar et al. 2022, 2025; Nayak et al. 2025).

In order to explore the possibility of the formation of a flux rope during flare evolution, we analyze the variations in photospheric magnetic flux near the fan of the 3D null (blue dashed box in Figure 5(a)). Relevantly, in panel (d) of Figure 6, we present temporal evolution of magnetic fluxes (both signed and unsigned) from 12:30 UT to 14:50 UT. Flux estimated by employing the LOS magnetograms from the data series `hmi.M_45s` (with a temporal cadence of $45s$) obtained from HMI/SDO. The panel shows the evolution of positive (blue curve), negative (orange curve) and total unsigned (green curve). It is crucial to highlight that no changes were observed in the magnetic fluxes during the hours leading up to the flare onset. However, following the flare onset at 13:50 UT, the negative flux begins to rise while the positive flux decreases until approximately 14:02 UT. As a result, the overall unsigned flux decreases throughout the flaring period, signifying the cancellation of magnetic fluxes within the region. It is notable that the cancellation of photospheric flux serves as a gradual process for the buildup of non-potential energy in that area (Fang et al. 2012; Kliem et al. 2021). Considering that the area for flux estimation corresponds to the fan footprint of the 3D null, the observations indicate a scenario in which the development of photospheric flux has played a role in building up magnetic stress and free magnetic energy directly within the magnetic arcades van Ballegooijen and Martens (1989). Importantly, the phenomenon of flux cancellation is frequently associated with the formation and growth of flux ropes (van Ballegooijen and Martens 1989; Green et al. 2011; Furuseth and Aulanier 2026; Wang et al. 2026). Taking into account the cancellation of magnetic flux in the region, we propose that the pink sheared field lines beneath the 3D null fan gradually transform into a magnetic flux rope over time during flare evolution, which may eventually erupt under suitable conditions.

Furthermore, to illustrate the morphological correlation between extrapolated field lines and the observed flare brightenings/ribbons, we superimpose the field lines with the AIA observations in Figure 7. Panel (a) displays the field lines overlaid on pre-flare observations from AIA 304 Å at 13:40 UT, indicating that the filament (pink lines)

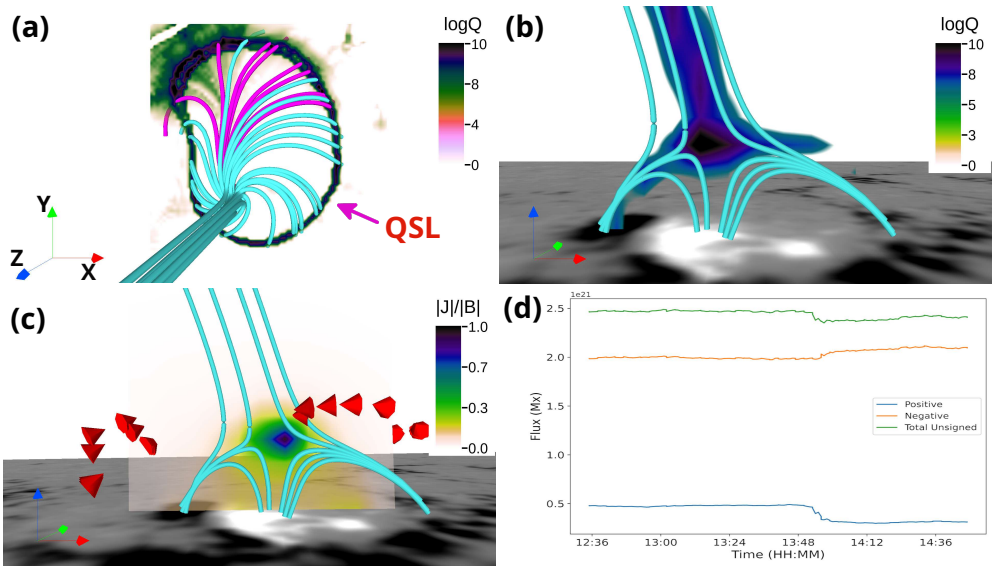


Fig. 6 Panel (a) of the figure shows the foot-points of fan of 3D null are anchored within the high $logQ$ region labeled as QSL1 (pink arrow). In panel (b) the field lines of the transverse field (derived by setting $B_y = 0$ in $\mathbf{B}$ for the cyan field lines), representing the projection of magnetic field lines on a y-constant plane and further overlaid with $logQ$. The panel (c) illustrates the field lines of transverse field are superimposed with $|\mathbf{J}|/|\mathbf{B}|$, representing the elevated value of $|\mathbf{J}|/|\mathbf{B}|$ at the neutral point. This corresponds to the increase in the gradient of the magnetic field at the neutral point and the red arrows in the panel shows the direction of L. Panel (d) plots the time evolution of the signed and unsigned photospheric magnetic fluxes in the vicinity of fan of 3D null.

located beneath the fan of the 3D null is co-located with the F (refer to Figure 2(a)). Next, in panel (b), the QSL identified at the bottom boundary is overplotted on the AIA 304 Å image at 13:55 UT. It is significant to note that the circular structure of the QSL1 nearly traces the BR1. In particular, the QSLs serve as the advantageous regions for the slipping reconnection where the magnetic field diffuses locally and progressively within the current layers that naturally form in the QSLs (Aulanier et al. 2006; Kumar et al. 2025). Consequently, we suggest that the onset of slipping reconnection under the suitable conditions within QSL1 significantly contributes to the emergence of the BR1 (Figure 2, 3). The panel (c) illustrate the the foot-points of the fan of the 3D null and spine closely align with the BR1 and BR2 (see Figure 2) appeared in AIA 304 Å at flare peak. This suggests the magnetic reconnection at 3D null is also contributing in the enhancement of BR1 and development of BR2. As shown earlier, there is strong gradient in field line connectivity in the vicinity of 3D null (see Figure 6(b)). In addition to this, the value of $|\mathbf{J}|/|\mathbf{B}|$ is elevated near the 3D null (refer to Figure 6(c)), which suggests a steep gradient of the magnetic field at the 3D null caused by the movement of non-parallel field lines in close proximity. This may result in the development of current sheet and potential onset of magnetic reconnection at 3D null as demonstrated in previous studies of Kumar et al. (2022, 2025); Nayak et al. (2025). The reconnection occurring at the 3D null accelerates charged particles

along its fan which significantly intensify the brightness of BR1 and R1 (Figures 2 and 3. Subsequently, the particles propelled along the spine field lines anchored in photosphere lead to the emergence of remote brightening BR2 and ribbon R2 (see Figures 2 and 3). Also, it is important to highlight that this fan-spine configuration resembles the coronal loops seen in the AIA 131 Å image (Figure 3(c)).

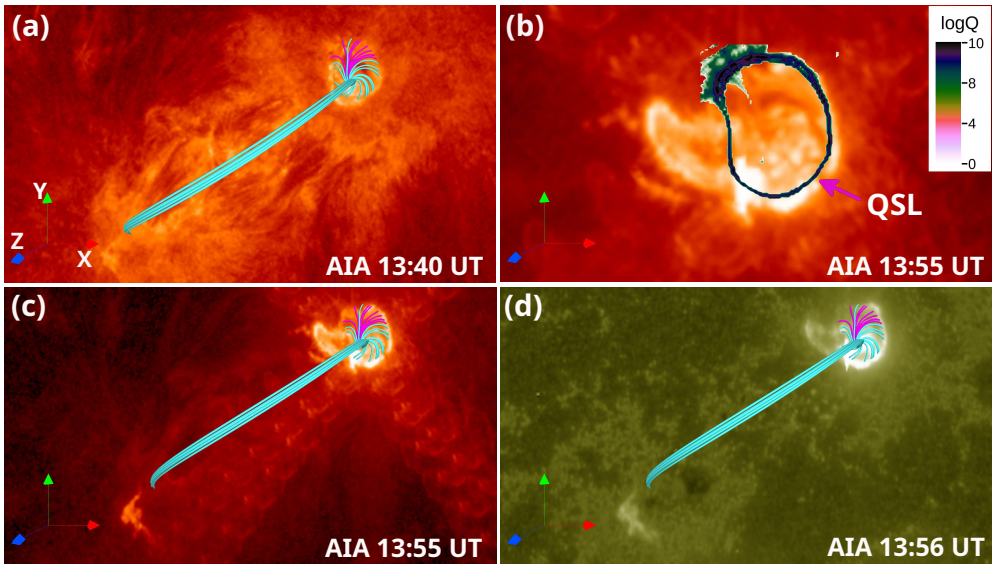


Fig. 7 Figure shows the morphological correlation between the extrapolated field lines and the AIA observations of the flare. Panel (a) illustrates the pink field lines are nearly co-spatial with the dark structure identified in pre-flare observation in AIA 304 Å image. Panel (b) plots the QSL over the AIA 304 Å observation at the flare peak— indicating circular structure of QSL co-aligns the circular brightening. Panel (c) and (d) present the foot-points of fan and spine of 3D null nearly co-spatial with the BR1/R1 and BR2/R2 appeared at flare and peak in AIA 304 Å and 1600 Å, highlighting the role of reconnection at 3D null in the development of flare brightenings/ribbons.

5 Summary and Discussion

In this work, we explore the onset mechanism of an X1.5-class solar flare that took place in NOAA AR 13006 on 10 May 2022, utilizing multi-wavelength observations from AIA/SDO and GONG Hα, in conjunction with a NFFF extrapolation of the coronal magnetic field. As the flare initiates we observe a subtle brightening in AIA 131 Å image which grows as a circular flare brightening (BR1) during the impulsive phase of the flare and shows its clear counter part in 304 Å. Subsequently, a remote brightening (BR2) appears in the southwest of BR1 in AIA 304 Å. These flare brightenings are identified as circular and remote ribbons (R1 and R2) in AIA 1600 Å images. Additionally, the GONG Hα observations indicate the existence of an arc-shaped filament prior to the flare commencement, which remains stable during the flare evolution and erupts after its conclusion of flare.

The NFFF extrapolation reconstructs a fan-spine magnetic topology that includes a 3D magnetic null point, with the filament situated beneath the fan dome. The extrapolated fan-spine configuration closely mirrors the coronal loop structure which is observed close to flare peak in AIA 131 Å image. Additionally, the fan footprints align with a circular QSL that spatially corresponds to the observed BR1 and R1, suggesting that the magnetic reconnection in QSL have played a significant role in the development of BR1 and R1. Also, the strong gradient in the field lines mapping (high $logQ$), and the exalted values of $|\mathbf{J}|/|\mathbf{B}|$ near the null point, along with a non-zero Lorentz force at lower coronal heights, indicate conducive conditions for the development of current sheets and the initiation of magnetic reconnection at the null.

Furthermore, the evolution of photospheric magnetic flux with time, indicates that flux cancellation occurs beneath the fan footprints during the flare evolution. Since no pre-existing magnetic flux rope is detected through twist analysis within the flaring region, the observed flux cancellation implies a gradual buildup of magnetic free energy and the potential transformation of the embedded filament into a flux rope that eventually erupts under the favorable conditions following the flare. It is significant to highlight that the continuous magnetic reconnection occurring in the overlying 3D null may play a role in reducing the strapping magnetic confinement above and facilitating the eruption.

Drawing from both observational data and magnetic topology analyses, we purpose a two-stage magnetic reconnection model for this event. The flare is likely triggered by slipping magnetic reconnection within the circular QSL, leading to the BR1. As magnetic stress escalates, reconnection occurs at the 3D null point, propelling particles along both the fan and spine field lines. This mechanism intensifies the BR1 and R1, while concurrently generating the BR2 and R2. The close correlation between the extrapolated magnetic topology and the observed flare morphology illustrates that both the QSL and the 3D null point are integral to the initiation and progression of this X1.5-class circular-ribbon flare. These findings underscore the necessity of considering interconnected reconnection processes involving QSLs and magnetic nulls to comprehend energy release in intricate solar flares.

In future we aim to perform a MHD simulation for the advancement of presented work. We also intend to gain insights into the calculation of the free magnetic energy available for flare emissions, as well as the contribution of this released free magnetic energy to both the thermal and non-thermal components.

Acknowledgements

We acknowledge the use of the visualization software VAPOR (www.vapor.ucar.edu) for generating relevant graphics. The computations were performed on high performance computer of Department of Physics, Patna University, Patna, India. Data and images are courtesy of NASA/SDO and the HMI and AIA science teams. AIA, HMI/SDO are joint efforts of many teams and individuals to whom we are greatly indebted for providing the data.

Declarations

Author contributions P.K., D.K and S.K. analyze the observations and extrapolation data. P.K. and D.K prepared the plots. P.K. and S.K. wrote the main draft of the paper. S.K, P.K and A.R.T contributed to the interpretation of the results. All authors did a careful proofreading of the text and improved the quality of the paper.

Funding Declaration S.K. and S. acknowledge financial support from the Anusandhan National Research Foundation (ANRF) - Science and Engineering Research Board (SERB) under Project No. SUR/2022/000569. S.K. also acknowledges financial support from Patna University under Project No. RDC/MRP/07.

Data Availability The data that support the findings of this study are available from the corresponding author upon reasonable request.

Competing interests The authors have no relevant financial or non-financial interests.

References

Agarwal, S., Bhattacharyya, R., Yang, S.: Study of Reconnection Dynamics and Plasma Relaxation in MHD Simulation of a Solar Flare. Solar Physics **299**(2), 15 (2024) https://doi.org/10.1007/s11207-024-02255-5 arXiv:2401.11417 [astro-ph.SR]

Aulanier, G., DeLuca, E.E., Antiochos, S.K., McMullen, R.A., Golub, L.: The Topology and Evolution of the Bastille Day Flare. ApJ **540**(2), 1126–1142 (2000) https://doi.org/10.1086/309376

Aulanier, G., Pariat, E., Démoulin, P., Devore, C.R.: Slip-Running Reconnection in Quasi-Separatrix Layers. Solar Physics **238**(2), 347–376 (2006) https://doi.org/10.1007/s11207-006-0230-2

Aschwanden, M.J., Shimizu, T.: Multi-wavelength Observations of the Spatio-temporal Evolution of Solar Flares with AIA/SDO. II. Hydrodynamic Scaling Laws and Thermal Energies. ApJ **776**(2), 132 (2013) https://doi.org/10.1088/0004-637X/776/2/132 arXiv:1308.5198 [astro-ph.SR]

Boerner, P., Edwards, C., Lemen, J., Rausch, A., Schrijver, C., Shine, R., Shing, L., Stern, R., Tarbell, T., Title, A., Wolfson, C.J., Soufli, R., Spiller, E., Gullikson, E., McKenzie, D., Windt, D., Golub, L., Podgorski, W., Testa, P., Weber, M.: Initial Calibration of the Atmospheric Imaging Assembly (AIA) on the Solar Dynamics Observatory (SDO). Solar Physics **275**(1-2), 41–66 (2012) https://doi.org/10.1007/s11207-011-9804-8

Bhattacharyya, R., Janaki, M.S., Dasgupta, B., Zank, G.P.: Solar Arcades as Possible

Minimum Dissipative Relaxed States. Solar Physics **240**(1), 63–76 (2007) https://doi.org/10.1007/s11207-006-0280-5

Berger, M.A., Prior, C.: The writhe of open and closed curves. Journal of Physics A Mathematical General **39**(26), 8321–8348 (2006) https://doi.org/10.1088/0305-4470/39/26/005

Carmichael, H.: A Process for Flares. In: Hess, W.N. (ed.) NASA Special Publication vol. 50, p. 451. unknown, ??? (1964)

Devi, P., Joshi, B., Chandra, R., Mitra, P.K., Veronig, A.M., Joshi, R.: Development of a Confined Circular-Cum-Parallel Ribbon Flare and Associated Pre-Flare Activity. Solar Physics **295**(6), 75 (2020) https://doi.org/10.1007/s11207-020-01642-y arXiv:2005.09586 [astro-ph.SR]

Furuseth, S.V., Aulanier, G.: Flux rope formation through flux cancellation of sheared coronal arcades in a 3D convectively driven MHD simulation. A&A **706**, 350 (2026) https://doi.org/10.1051/0004-6361/202554242 arXiv:2512.20716 [astro-ph.SR]

Fletcher, L., Dennis, B.R., Hudson, H.S., Krucker, S., Phillips, K., Veronig, A., Battaglia, M., Bone, L., Caspi, A., Chen, Q., Gallagher, P., Grigis, P.T., Ji, H., Liu, W., Milligan, R.O., Temmer, M.: An Observational Overview of Solar Flares. Space Science Reviews **159**(1-4), 19–106 (2011) https://doi.org/10.1007/s11214-010-9701-8 arXiv:1109.5932 [astro-ph.SR]

Fang, F., Manchester, W. IV, Abbett, W.P., van der Holst, B.: Buildup of Magnetic Shear and Free Energy during Flux Emergence and Cancellation. ApJ **754**(1), 15 (2012) https://doi.org/10.1088/0004-637X/754/1/15 arXiv:1205.3764 [astro-ph.SR]

Gary, G.A.: Plasma Beta above a Solar Active Region: Rethinking the Paradigm. Solar Physics **203**(1), 71–86 (2001) https://doi.org/10.1023/A:1012722021820

Gary, G.A., Hagyard, M.J.: Transformation of vector magnetograms and the problems associated with the effects of perspective and the azimuthal ambiguity. Solar Physics **126**, 21–36 (1990) https://doi.org/10.1007/BF00158295

Green, L.M., Kliem, B., Wallace, A.J.: Photospheric flux cancellation and associated flux rope formation and eruption. A&A **526**, 2 (2011) https://doi.org/10.1051/0004-6361/201015146 arXiv:1011.1227 [astro-ph.SR]

Gong, L., Yan, X., Liang, H., Xue, Z., Wang, J., Yang, L., Peng, Y., Yang, L., Zhang, X.: Rearrangement of sunspot magnetic field caused by an X1.5 solar flare. MNRAS **530**(4), 3897–3905 (2024) https://doi.org/10.1093/mnras/stae1020

Hu, Q., Dasgupta, B.: An Improved Approach to Non-Force-Free Coronal Magnetic Field Extrapolation. Solar Physics **247**(1), 87–101 (2008) https://doi.org/10.1007/

s11207-007-9090-7

Hu, Q., Dasgupta, B., Choudhary, D.P., Büchner, J.: A Practical Approach to Coronal Magnetic Field Extrapolation Based on the Principle of Minimum Dissipation Rate. ApJ **679**(1), 848–853 (2008) https://doi.org/10.1086/587639 arXiv:0711.1376 [astro-ph]

Hu, Q., Dasgupta, B., Derosa, M.L., Büchner, J., Gary, G.A.: Non-force-free extrapolation of solar coronal magnetic field using vector magnetograms. Journal of Atmospheric and Solar-Terrestrial Physics **72**(2-3), 219–223 (2010) https://doi.org/10.1016/j.jastp.2009.11.014

Hirayama, T.: Theoretical Model of Flares and Prominences. I: Evaporating Flare Model. Solar Physics **34**(2), 323–338 (1974) https://doi.org/10.1007/BF00153671

Haynes, A.L., Parnell, C.E.: A trilinear method for finding null points in a three-dimensional vector space. Physics of Plasmas **14**(8), 082107–082107 (2007) https://doi.org/10.1063/1.2756751 arXiv:0706.0521 [astro-ph]

Joshi, R., Mandrini, C.H., Chandra, R., Schmieder, B., Cristiani, G.D., Mac Cormack, C., Démoulin, P., Cremades, H.: Analysis of the Evolution of a Multi-Ribbon Flare and Failed Filament Eruption. Solar Physics **297**(7), 81 (2022) https://doi.org/10.1007/s11207-022-02021-5 arXiv:2206.00531 [astro-ph.SR]

Kumar, S., Kumar, P., Sadashiv, Nayak, S.S., Agarwal, S., Prasad, A., Bhattacharyya, R., Chandra, R.: Data-Constrained Magnetohydrodynamics Simulation of a Confined X-Class Flare in NOAA Active Region 11166. Solar Physics **300**(2), 22 (2025) https://doi.org/10.1007/s11207-025-02426-y arXiv:2501.11066 [astro-ph.SR]

Kliem, B., Lee, J., Liu, R., White, S.M., Liu, C., Masuda, S.: Nonequilibrium Flux Rope Formation by Confined Flares Preceding a Solar Coronal Mass Ejection. ApJ **909**(1), 91 (2021) https://doi.org/10.3847/1538-4357/abda37 arXiv:2101.02181 [astro-ph.SR]

Kumar, S., Nayak, S.S., Prasad, A., Bhattacharyya, R.: Magnetic Reconnections in the Presence of Three-Dimensional Magnetic Nulls and Quasi-Separatrix Layers. Solar Physics **296**(1), 26 (2021) https://doi.org/10.1007/s11207-021-01768-7 arXiv:2101.02065 [astro-ph.SR]

Kopp, R.A., Pneuman, G.W.: Magnetic reconnection in the corona and the loop prominence phenomenon. Solar Physics **50**(1), 85–98 (1976) https://doi.org/10.1007/BF00206193

Kumar, S., Prasad, A., Sarkar, R., Bhattacharyya, R.: Magnetohydrodynamics evolution of three-dimensional magnetic null in NOAA active region 11515 initiated using non-force-free field extrapolation. Frontiers in Astronomy and Space Sciences **9**, 1039061 (2022) https://doi.org/10.3389/fspas.2022.1039061 arXiv:2210.03957

[astro-ph.SR]

Kumar, P., Sadashiv, Kumar, S., Nayak, S.S., Kaur, S., Bhattacharya, R.: Magnetic Reconnection at Hyperbolic Flux Tube associated with a Confined Flare in NOAA Active Region 12268 (2026). https://arxiv.org/abs/2604.10684

Liu, R., Kliem, B., Titov, V.S., Chen, J., Wang, Y., Wang, H., Liu, C., Xu, Y., Wiegelmann, T.: Structure, Stability, and Evolution of Magnetic Flux Ropes from the Perspective of Magnetic Twist. ApJ **818**(2), 148 (2016) https://doi.org/10.3847/0004-637X/818/2/148 arXiv:1512.02338 [astro-ph.SR]

Li, T., Liu, L., Hou, Y., Zhang, J.: Two Types of Confined Solar Flares. ApJ **881**(2), 151 (2019) https://doi.org/10.3847/1538-4357/ab3121 arXiv:1907.04510 [astro-ph.SR]

Lemen, J.R., Title, A.M., Akin, D.J., Boerner, P.F., Chou, C., Drake, J.F., Duncan, D.W., Edwards, C.G., Friedlaender, F.M., Heyman, G.F., Hurlburt, N.E., Katz, N.L., Kushner, G.D., Levay, M., Lindgren, R.W., Mathur, D.P., McFeaters, E.L., Mitchell, S., Rehse, R.A., Schrijver, C.J., Springer, L.A., Stern, R.A., Tarbell, T.D., Wuelser, J.-P., Wolfson, C.J., Yanari, C., Bookbinder, J.A., Cheimets, P.N., Caldwell, D., Deluca, E.E., Gates, R., Golub, L., Park, S., Podgorski, W.A., Bush, R.I., Scherrer, P.H., Gummin, M.A., Smith, P., Auker, G., Jerram, P., Pool, P., Soufli, R., Windt, D.L., Beardsley, S., Clapp, M., Lang, J., Waltham, N.: The Atmospheric Imaging Assembly (AIA) on the Solar Dynamics Observatory (SDO). Solar Physics **275**(1-2), 17–40 (2012) https://doi.org/10.1007/s11207-011-9776-8

Mandrini, C.H., Démoulin, P., Van Driel-Gesztelyi, L., Schmieder, B., Cauzzi, G., Hofmann, A.: 3D Magnetic Reconnection at an X-Ray Bright Point. Solar Physics **168**(1), 115–133 (1996) https://doi.org/10.1007/BF00145829

Metcalf, T.R., Jiao, L., McClymont, A.N., Canfield, R.C., Uitenbroek, H.: Is the Solar Chromospheric Magnetic Field Force-free? ApJ **439**, 474 (1995) https://doi.org/10.1086/175188

Masson, S., Pariat, E., Aulanier, G., Schrijver, C.J.: The Nature of Flare Ribbons in Coronal Null-Point Topology. ApJ **700**(1), 559–578 (2009) https://doi.org/10.1088/0004-637X/700/1/559

Nayak, S.S., Bhattacharyya, R., Prasad, A., Hu, Q., Kumar, S., Joshi, B.: A Data-constrained Magnetohydrodynamic Simulation of Successive Events of Blowout Jet and C-class Flare in NOAA AR 12615. ApJ **875**(1), 10 (2019) https://doi.org/10.3847/1538-4357/ab0a0b

Nayak, S.S., Bhattacharyya, R., Smolarkiewicz, P.K., Kumar, S., Prasad, A.: On the Spontaneous Generation of Three-dimensional Magnetic Nulls. ApJ **892**(1), 44 (2020) https://doi.org/10.3847/1538-4357/ab75bb

Nayak, S.S., Hu, Q., He, W., Kumar, S., Bhattacharyya, R.: On the Magnetic Reconnection and Its Properties During a Flare Using a Magnetohydrodynamics Simulation. Solar Physics **300**(6), 79 (2025) https://doi.org/10.1007/s11207-025-02492-2 arXiv:2505.11186 [astro-ph.SR]

O'Dwyer, B., Del Zanna, G., Mason, H.E., Weber, M.A., Tripathi, D.: SDO/AIA response to coronal hole, quiet Sun, active region, and flare plasma. A&A **521**, 21 (2010) https://doi.org/10.1051/0004-6361/201014872

Olshevsky, V., Pontin, D.I., Williams, B., Parnell, C.E., Fu, H.S., Liu, Y., Yao, S., Khotyaintsev, Y.V.: A comparison of methods for finding magnetic nulls in simulations and in situ observations of space plasmas. A&A **644**, 150 (2020) https://doi.org/10.1051/0004-6361/202039182 arXiv:2101.02014 [physics.space-ph]

Prasad, A., Bhattacharyya, R., Hu, Q., Kumar, S., Nayak, S.S.: A Magnetohydrodynamic Simulation of Magnetic Null-point Reconnections in NOAA AR 12192, Initiated with an Extrapolated Non-force-free Field. ApJ **860**(2), 96 (2018) https://doi.org/10.3847/1538-4357/aac265 arXiv:1805.00635 [astro-ph.SR]

Prasad, A., Dissauer, K., Hu, Q., Bhattacharyya, R., Veronig, A.M., Kumar, S., Joshi, B.: Magnetohydrodynamic Simulation of Magnetic Null-point Reconnections and Coronal Dimmings during the X2.1 Flare in NOAA AR 11283. ApJ **903**(2), 129 (2020) https://doi.org/10.3847/1538-4357/abb8d2 arXiv:2009.11109 [astro-ph.SR]

Prasad, A., Kumar, S., Sterling, A.C., Moore, R.L., Aulanier, G., Bhattacharyya, R., Hu, Q.: Formation of an observed eruptive flux rope above the torus instability threshold through tether-cutting magnetic reconnection. A&A **677**, 43 (2023) https://doi.org/10.1051/0004-6361/202346267 arXiv:2307.06572 [astro-ph.SR]

Priest, E.: Magnetic reconnection on the Sun: ESPD Senior Prize Lecture. Advances in Space Research **71**(4), 1856–1865 (2023) https://doi.org/10.1016/j.asr.2022.03.028

Pesnell, W.D., Thompson, B.J., Chamberlin, P.C.: The Solar Dynamics Observatory (SDO). Solar Physics **275**(1-2), 3–15 (2012) https://doi.org/10.1007/s11207-011-9841-3

Shibata, K., Magara, T.: Solar Flares: Magnetohydrodynamic Processes. Living Reviews in Solar Physics **8**(1), 6 (2011) https://doi.org/10.12942/lrsp-2011-6

Schou, J., Scherrer, P.H., Bush, R.I., Wachter, R., Couvidat, S., Rabello-Soares, M.C., Bogart, R.S., Hoeksema, J.T., Liu, Y., Duvall, T.L., Akin, D.J., Allard, B.A., Miles, J.W., Rairden, R., Shine, R.A., Tarbell, T.D., Title, A.M., Wolfson, C.J., Elmore, D.F., Norton, A.A., Tomczyk, S.: Design and Ground Calibration of the Helioseismic and Magnetic Imager (HMI) Instrument on the Solar Dynamics Observatory (SDO). Solar Physics **275**(1-2), 229–259 (2012) https://doi.org/10.1007/s11207-011-9842-2

Sturrock, P.A.: Model of the High-Energy Phase of Solar Flares. Nature **211**(5050),

695–697 (1966) https://doi.org/10.1038/211695a0

Titov, V.S., Démoulin, P.: Basic topology of twisted magnetic configurations in solar flares. A&A **351**, 707–720 (1999)

Titov, V.S., Hornig, G., Démoulin, P.: Theory of magnetic connectivity in the solar corona. Journal of Geophysical Research (Space Physics) **107**(A8), 1164 (2002) https://doi.org/10.1029/2001JA000278

van Ballegooijen, A.A., Martens, P.C.H.: Formation and Eruption of Solar Prominences. ApJ **343**, 971 (1989) https://doi.org/10.1086/167766

Wiegelmann, T.: Nonlinear force-free modeling of the solar coronal magnetic field. Journal of Geophysical Research (Space Physics) **113**(A3), 03–02 (2008) https://doi.org/10.1029/2007JA012432 arXiv:0801.2902 [astro-ph]

Wang, H., Liu, C.: Circular Ribbon Flares and Homologous Jets. ApJ **760**(2), 101 (2012) https://doi.org/10.1088/0004-637X/760/2/101 arXiv:1207.7345 [astro-ph.SR]

Wang, D., Liu, R., Wang, Y., Liu, K., Chen, J., Liu, J., Zhou, Z., Zhang, M.: Critical Height of the Torus Instability in Two-ribbon Solar Flares. ApJL **843**(1), 9 (2017) https://doi.org/10.3847/2041-8213/aa79f0 arXiv:1706.03169 [astro-ph.SR]

Wiegelmann, T., Sakurai, T.: Solar Force-free Magnetic Fields. Living Reviews in Solar Physics **9**(1), 5 (2012) https://doi.org/10.12942/lrsp-2012-5

Wang, C., Yokoyama, T., Chen, F., Xing, C., Ding, M., Lu, Z.: Formation of a Magnetic Flux Rope prior to the Eruption: Insight from a Radiative MHD Simulation of Active Region Emergence. ApJL **996**(2), 35 (2026) https://doi.org/10.3847/2041-8213/ae2d57 arXiv:2512.14348 [astro-ph.SR]

Wang, Y., Zhang, J.: A Comparative Study between Eruptive X-Class Flares Associated with Coronal Mass Ejections and Confined X-Class Flares. ApJ **665**(2), 1428–1438 (2007) https://doi.org/10.1086/519765 arXiv:0808.2976 [astro-ph]

Yang, S., Zhang, J., Xiang, Y.: Fine Structures and Overlying Loops of Confined Solar Flares. ApJL **793**(2), 28 (2014) https://doi.org/10.1088/2041-8205/793/2/L28 arXiv:1409.0471 [astro-ph.SR]